Real-Time Dynamic Behavior Evaluation of Active Distribution Networks Leveraging Low-Cost PMUs

Xuejun Zheng, Shaorong Wang *, Xin Su, Mengmeng Xiao, Zia Ullah [ID], Xin Hu and Chang Ye

School of Electrical and Electronic Engineering, Huazhong University of Science and Technology, Wuhan 430074, China; xuejun.zheng@foxmail.com (X.Z.); d201780389@hust.edu.cn (X.S.); d201577332@hust.edu.cn (M.X.); ziaullah@hust.edu.cn (Z.U.); m202071484@hust.edu.cn (X.H.); M201971391@hust.edu.cn (C.Y.)
* Correspondence: wsrwy96@vip.sina.com

Abstract: The investigation of real-time dynamic behavior evaluation in the active distribution networks (ADNs) is a challenging task, and it has great importance due to the emerging trend of distributed generations, electric vehicles, and flexible loads integration. The advent of new elements influences the dynamic behavior of the electric distribution networks and increases the assessment complexity. However, the proper implementation of low-cost phasor measurement units (PMUs) together with the development of power system applications offer tremendous benefits. Therefore, this paper proposes a PMU-based multi-dimensional dynamic index approach for real-time dynamic behavior evaluation of ADNs. The proposed evaluation model follows the assessment principles of accuracy, integrity, practicability, and adaptability. Additionally, we introduced low-cost PMUs in the assessment model and implemented them for real-time and high-precision monitoring of dynamic behaviors in the entire distribution network. Finally, a complete model called the real-time dynamic characteristics evaluation system is presented and applied to the ADN. It is pertinent to mention that our proposed evaluation methodology does not rely on the network topology or line parameters of the distribution network since only the phasor measurements of node voltage and line current are involved in the dynamic index system. Thus, the presented methodology is well adaptive to different operation states of ADN despite frequent topology changes. The validation of the proposed approach was verified by conducting simulations on the modified IEEE 123-node distribution network. The obtained results verify the effectiveness and relevance of the proposed model for the real-time dynamic behavior evaluation of ADNs.

Keywords: active distribution network; dynamic index; dynamic characteristics assessment; low-cost PMUs

1. Introduction

The real-time dynamic behavior assessment of active distribution networks (ADNs) is one of the important aspects and is to be considered due to the modern advancements in electric power systems. The dynamic behavior assessment involves various factors such as over-limits, oscillation, short-time impact, and other situations that appear in the entire distribution network. The complexity of the assessment and evaluation process rises due to the integration of new elements in the system. As reported in the reference [1–3], compared with the traditional distribution network, the behavior of the modern ADNs is highly uncertain due to the growing penetration of distributed generations (DGs), electric vehicles (EVs), and flexible loads. Especially in such a situation, the dynamic process and evaluation become more complicated due to the varying operating conditions [4–6]. In terms of operating conditions, the intermittent and stochastic traits of renewable energy sources (RES) entail predictions upon distribution network power flow increasingly challenging [7–9]. Moreover, the load characteristics of the distribution network present new alterations, such as the impulse grid to vehicle (G2V) mode and the mobile vehicle to grid (V2G).

Since the probability of dynamic behavior of the ADN is much uncertain than the traditional distribution networks, several studies have been conducted concerning the ADN assessment for the optimization of various technical and economic aspects. To deal with the highly uncertain behavior and dynamic disturbances of the ADN, reference [10] proposed a novel node flexibility evaluation methodology for the assessment of ADN parameters that enhance the flexibility of nodes compared with other techniques. Highlighting the importance of distribution networks evaluation in reference [11], an autoencoder-based method is presented to accurately evaluate the voltage stability of the power system. In reference [12], the importance of reliability assessment for ADN was addressed, and a comprehensive survey on reliability assessment techniques for modern ADN is presented. Applying the same note of reliability assessment of ADN, an analytical approach has been developed in [13] to assess the influence of energy storage on reliability. The study of distribution network evaluation mainly focuses on evaluating the reliability, economy, and development of the network over a long time from the perspective of planning and construction [14,15]. Even when assessing the operating status, the corresponding estimation indexes mainly concern the statistical results of bus voltage and branch power flow in a duration of time rather than the indication of their real-time changes.

Besides, since the topology and dynamic characteristics of the ADN have undergone profound changes, and become dramatically complex, the conventional supervisory control and data acquisition (SCADA) is far from meeting the requirements of real-time and high-precision dynamic process monitoring of ADN [16]. Fortunately, with the advent of high sampling-rate, high-resolution, and high-accuracy phasor measurement unit (PMU) in the ADNs, the study on its development and various possible applications have been in the spotlight [17,18], such as topology detection [19], line parameter estimation [20], fault location [21], and three-phase unbalance mitigation combing with 5G (5th generation wireless network) network [22]. However, the high cost impedes the extensive exploitation of PMUs in ADN. Thus, it is an increasing tendency to develop and implement low-cost and high-precision PMUs for dynamic behavior monitoring in the ADNs, and generally, the DFT (discrete Fourier transformation)-based method was introduced and improved for low-cost PMUs [23,24].

In view of the above literature, it has been found that rare studies are available concerning the assessment of dynamic characteristics of the modern ADN. Indeed, DGs, EVs, energy storage devices, and even flexible loads in ADN have their feedback control systems. The dynamic characteristics and interactions of these feedback control systems may deteriorate the dynamic process of ADN, such as the frequent over-limits and continuous power oscillation of the bus voltage or branch current. Considering the challenge of uncertain and dynamic characteristics evaluation of ADN, this paper originates a low-cost PMUs-based evaluation model to accurately perform the assessment of real-time dynamic behavior. The assessment is conducted via three main steps. First, the non-DFT method is developed for the extensive allocation of PMUs in the ADN at a low cost. Second, the dynamic characteristics evaluation index of ADN is established in terms of node voltage and branch current or power flow. Later, the dynamic characteristics evaluation methodology of ADN is implemented based on the widely allocated low-cost PMUs and the constructed comprehensive indexes. Considering the aforementioned dynamic process in the ADN, the proposed method is expected to evaluate the dynamic characteristics of ADN thoroughly with high precision and further applied to the dynamic characteristics improvement, the operation optimization, and the planning and design projects refinement in the ADN.

The main novelties and contributions of this paper are listed as follows:

(1) As per our knowledge and the available literature, the present study reports for the first time the application of low-cost PMUs in the real-time dynamic behavior evaluation of ADNs. We present a novel approach to obtain the voltage amplitude based on the full-wave rectifier with no need for expensive ADC and microprocessor chips.

(2) Propose a novel and comprehensive dynamic index system to evaluate the dynamic characteristics of ADNs, following a multi-level progression of node-branch-subarea-network.

(3)   Present a low-cost PMUs enabled real-time dynamic behavior evaluation methodology of ADNs based on the proposed comprehensive index system. The proposed approach can adapt to various operating conditions and is agnostic to the network topology or line parameters.

The rest of this paper is structured as follows. In Section 2, the low-cost PMU is developed based on a non-DFT method and offers opportunities for real-time and high-precision monitoring of the whole network at an acceptable cost. Section 3 introduces the guidelines for the real-time assessment of the ADN's dynamic characteristics and presents a dynamic index system based on the node voltage and branch current and power flow in the ADN. Furthermore, we propose a real-time evaluation methodology of dynamic characteristics in Section 4. In Section 5, the numerical tests are conducted for the method verification using the modified IEEE 123-node distribution network. Finally, we conclude the paper in Section 6.

2. The Non-DFT Method Developed for Low-Cost PMUs

For large exploitation of PMUs in the ADN, we focus on the development and phasor measurement method of low-cost PMUs and proposed a non-DFT-based methodology. The frequency and phase of the voltage phasor are acquired by the signal zero-crossing detection method [25], while the amplitude is obtained after being processed in the full-wave rectifier. The phase shift of the filter and the shaping circuit can be compensated by software.

The schematic design diagram of a low-cost PMU device based on the non-DFT method is shown in Figure 1.
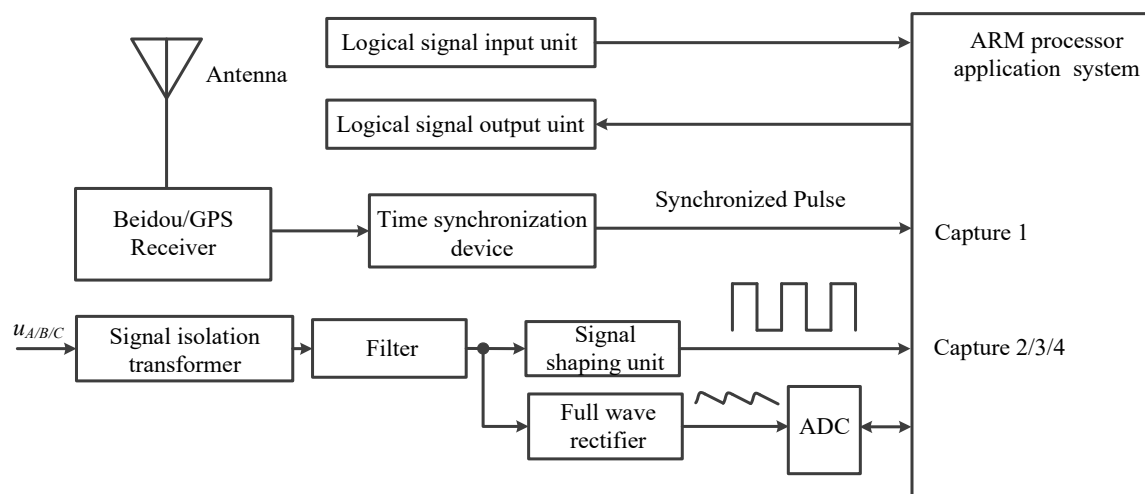

Figure 1. The schematic diagram of the proposed low-cost PMU based on the non-DFT method.

As indicated in Figure 1, the three-phase voltage-measured signals u_A, u_B, and u_C are being isolated, transformed, and filtered, respectively. Subsequently, only the base-frequency voltage signal is transformed into a DC voltage signal with a small unidirectional ripple by the full-wave rectifier and input to the A/D (analog to digital) conversion module to be processed by the microprocessor further. By sampling the DC voltage signal, the microprocessor can get the average value in the signal period, and then the amplitude of the measured voltage signal is obtained. A simple circuit can implement this method with high precision and small-quantity computation.

The designed full-wave rectifier circuit is shown in Figure 2a. The operational amplifier is OP07, diodes D_1–D_5 are 1N4007, the value of the input resistance R_1 and the operational amplifier input and output resistances R_2–R_4 are 10 kΩ, while R_5 is 100 Ω. The measured voltage signal u_s is rectified into a one-way full-wave rectified voltage signal u_{sq} through an operational amplifier circuit. u_{sq} is the combination of the positive half of us and the phase

reversed negative half of u_s. u_{sq} is a DC full-wave voltage signal with large pulsations. When the resistive load R is connected in parallel with a filter capacitor C, the output voltage u_o, which is originally a full-wave DC voltage waveform with large pulsation, will be smoothed. The pulsation component will be reduced, and the average value of output voltage u_o will be improved, as indicated in Figure 2b.
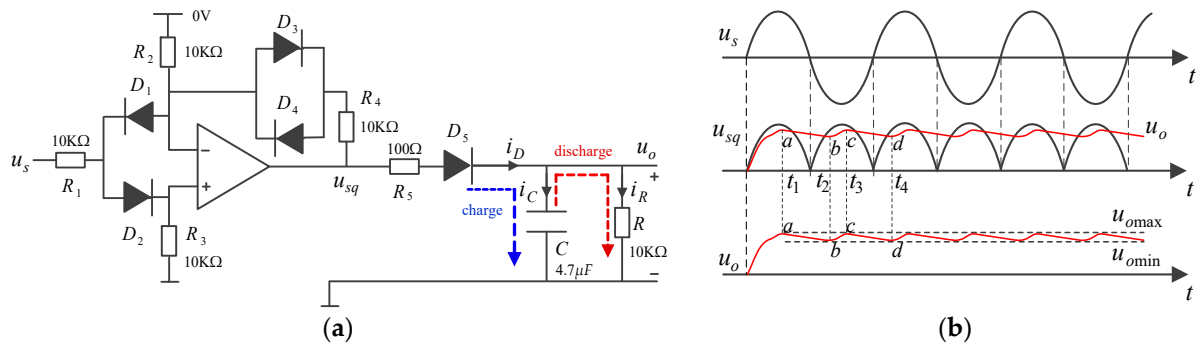
Figure 2. Full-wave rectifying circuit and its output voltage: (**a**) the designed full-wave rectifying circuit; (**b**) the diagram of output voltage during the charge/discharge process of filter capacitor.

The proposed non-DFT-based PMUs device can achieve high-precision measurement of three-phase frequency, phase, and amplitude parameters of voltage and current phasors even when the frequency is offset. It has the advantage of low cost with no need for expensive ADC and microprocessor chips. Thus, it is feasible to widely allocate the PMU devices at each node, enabling the observation and evaluation of dynamic characteristics across the whole distribution network.

For the parameter of the resistor R and capacitor C of the above full-wave rectifier-capacitor filter circuit, the values are generally determined according to the following equation.

$$RC = (3 \sim 5)T/2 \tag{1}$$

where T is the period of the measured voltage signal u_s, and the value of T is 20 ms for the fundamental signal. In the designed circuit, the value of R is 10 kΩ while the value of C is 4.7 μF. Assuming that the amplitude of u_s is U_m, the withstand voltage of both the rectifier diode and the filter capacitor should be greater than U_m.

Assuming that the $N + 1$ sampling points before the synchronous measurement time are $f(0), f(1), f(2), \dots, f(N-2), f(N-1), f(N)$, then the sampled average value of output voltage u_o over one cycle of the measured signal is:

$$U_{oav} = \frac{\sum\limits_{i=0}^{N-1} f(i) + m \times f(N)}{N_T} \tag{2}$$

The average value U_{oav} of the output voltage u_o after filtering by the full-wave rectifier capacitor conforms to the following equation:

$$U_{oav} = \sqrt{2}U_2\left(1 - \frac{T}{4RC}\right) = U_m\left(1 - \frac{T}{4RC}\right) \tag{3}$$

where U_2 is the root-mean-square (RMS) value of the measured voltage signal u_s.

Thus, U_m can be expressed as follows:

$$U_m = U_{oav}/\left(1 - \frac{T}{4RC}\right) = 1.119 \times U_{oav} \tag{4}$$

However, Formula (4) is the ideal relationship between U_m and U_{oav}. In practice, the conduction voltage drop of the diode is not zero, so U_m is not directly proportional to U_{oav}.

In this paper, measured signals of different amplitudes at 50 Hz are simulated, from which the fitted functional relationship between U_m and U_{oav} can be obtained as:

$$U_m = 1.117 \times U_{oav} + 0.4686 \tag{5}$$

Using Formula (5), the measured amplitude U_m' can be calculated. And the measurements and measurement errors of voltage magnitude are displayed in Table 1. According to Table 1, when U_m varies in the range of 3.0~6.0 V, the measured magnitude value U_m' calculated via the fitting function is very close to U_m, and the maximum relative error of the magnitude value is only 0.17%, indicating the high precision of the magnitude measurements.

**Table 1.** The magnitude measurements and errors.

U_m /V	U_{oav} /V	U_m' /V	Absolute Error /V	Relative Error /%	U_m /V	U_{oav} /V	U_m' /V	Absolute Error /V	Relative Error /%
3.0	2.264	2.9976	−0.0024	0.08	4.6	3.700	4.6016	0.0016	0.04
3.1	2.354	3.0981	−0.0019	0.06	4.7	3.790	4.7021	0.0021	0.05
3.2	2.443	3.1975	−0.0025	0.08	4.8	3.880	4.8026	0.0026	0.05
3.3	2.533	3.2980	−0.0020	0.06	4.9	3.970	4.9032	0.0032	0.06
3.4	2.622	3.3974	−0.0026	0.08	5.0	4.059	5.0026	0.0026	0.05
3.5	2.712	3.4980	−0.0020	0.06	5.1	4.150	5.1042	0.0042	0.08
3.6	2.801	3.5974	−0.0026	0.07	5.2	4.240	5.2048	0.0048	0.09
3.7	2.891	3.6979	−0.0021	0.06	5.3	4.331	5.3064	0.0064	0.12
3.8	2.981	3.7985	−0.0015	0.04	5.4	4.417	5.4025	0.0025	0.05
3.9	3.071	3.8990	−0.0010	0.03	5.5	4.510	5.5064	0.0064	0.12
4.0	3.160	3.9984	−0.0016	0.04	5.6	4.600	5.6069	0.0069	0.12
4.1	3.250	4.0989	−0.0011	0.03	5.7	4.690	5.7074	0.0074	0.13
4.2	3.340	4.1995	−0.0005	0.01	5.8	4.781	5.8091	0.0091	0.16
4.3	3.430	4.3000	0.0000	0.00	5.9	4.871	5.9096	0.0096	0.16
4.4	3.520	4.4005	0.0005	0.01	6.0	4.961	6.0101	0.0101	0.17
4.5	3.610	4.5010	0.0010	0.02					

Additionally, it can be seen from Formula (4) that the functional relationship between U_m and U_{oav} is relevant to T, i.e., it is related to the measured signal frequency f_s. In the case where R and C are fixed, the functional relationship between U_m and U_{oav} varies with f_s. When f_s is 45 Hz and the magnitude U_m ranges from 3.0 V to 6.0 V, the maximum relative error between U_m' and U_m is 0.31%; if f_s equals 55 Hz, the maximum relative error is 0.42%. It can be observed that the magnitude measurement error becomes larger. In order to decrease the magnitude measurement error, the fitted functional relationship between U_m and U_{oav} should be updated according to the measurements at corresponding f_s. In fact, the proposed non-DFT-based PMU can meet 0.5-class smart meter requirements (or even 0.2-class metering device requirements if necessary) when f_s varies within 45.0~55.0 Hz.

3. Construction of the Dynamic Index System

3.1. The Guidelines of Online Dynamic Characteristics Assessment of ADN Based on PMUs

Two possible dynamic trajectories of PMU data of ADNs within the observation time window are shown in Figure 3. Unlike the dynamic process of a second-order control system that always converges, the PMU data of an ADN is in the dynamic process at all times and may never converge. Still, by referring to the definition of the steady-state interval of the second-order control system, we can define the average value of the measurements in the observation time window as "equivalent steady-state value" and furthermore define its "equivalent balance interval", which will be described in detail in Sections 3.1 and 3.2.
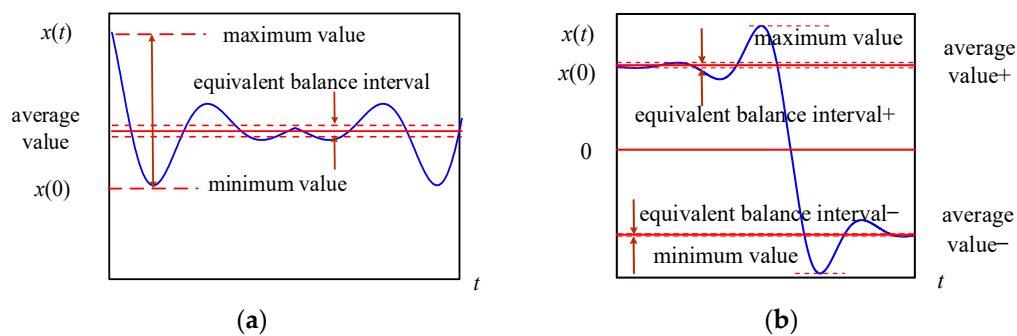
Figure 3. Dynamic trajectory schematic diagrams of PMU data of ADNs: (**a**) Dynamic trajectory 1; (**b**) dynamic trajectory 2.

Then, the real-time evaluation guidelines of ADN's dynamic characteristics are:

(1) Scientificity: The adverse dynamic process of ADN can be accurately identified by sufficiently considering the influence of distributed power, energy storage system, electric vehicle charging facilities, flexible load, and control system coupling on the dynamic process of ADN.

(2) Integrity: This methodology can estimate the fluctuation of local state variables in the dynamic process of ADN, and simultaneously comprehensively evaluate the dynamic characteristics of subareas and the entire system.

(3) Practicability: The evaluation index and model are supposed to be concise and speedy calculated online. The real-time cycle mode is adopted in the evaluation process, which can evaluate the dynamic characteristics of the present object in different time periods.

(4) Adaptability: Considering the frequent changes of the operation mode and topology structure of ADN, the assessment method should be capable of conducting real-time evaluation without the information of operating modes, network topology, or line parameters. For instance, while optimizing the dynamic characteristics of ADN by changing its topology or adopting additional control, the evaluation method should reflect the changes of the dynamic indexes before and after taking these measures in time, which can provide the basis for the dynamic characteristics optimization control.

It is worthy of notice that the data collected by PMUs can monitor the real-time dynamic process of ADN. The low-cost PMUs are developed and assumed installed at each node in this paper so that the observability is well implemented in the ADN.

The dynamic index system is built up for the ADN dynamic characteristics evaluation according to the aforementioned guiding ideology. The redundancy of the built-up dynamic index subset is needed taking into account the convenient usage of the dynamic index calculation results and the ability to describe the problem from multiple aspects, which means that some dynamic indexes are correlated or coupled. However, the correct evaluation results of ADN dynamic characteristics can be obtained by selecting a set of irrelevant or approximately irrelevant indicators according to the principle of completeness.

The built-up dynamic index set includes four parts: individual node dynamic index, individual branch dynamic index, subarea dynamic index, and whole network dynamic index, which will be introduced below.

3.2. Dynamic Index of Individual Node Voltage

The objective of the proposed dynamic index of node voltage is involved in two aspects:

(1) By computing the dynamic indexes of node voltage amplitude online, it is expected to find out whether the node voltage frequently exceeds the allowed limits in the dynamic process of the ADN, including the amplitude and frequency beyond the allowed limits as well as the percentage of time of the voltage limit violations.

(2) By calculating the dynamic indexes of instantaneous frequency and phase angle of node voltage online, it is expected to discover in time whether there are adverse dynamic processes such as periodic oscillation in the ADN.

3.2.1. Dynamic Index of Individual Node Voltage Amplitude

Assuming that the number of the voltage amplitude measurements at the node j in the present observation time window is N (note: the measurements include the data collected at the starting time of the time window $t = 0$, the sample time interval is ΔT, the length of the time window is $N\Delta T$, the $(N + 1)th$ data (presented by per unit value) can be observed but belongs to the following observation time window), the number of the sampled data point is noted as i, the average value at node j is $\overline{U}_j$ and expressed as $\overline{U}_j = \frac{1}{N} \sum\limits_{i=0}^{N-1} U_j(i)$, the corresponding "equivalent balance interval" is $\left[0.98\overline{U}_j, 1.02\overline{U}_j\right]$, the node rated voltage is U_{jN} and its rated voltage magnitude is expressed as $U_{jNm} = \sqrt{2}U_{jN}$, the normal range of U_{jNm} is $\left[0.98U_{jNm}, 1.02U_{jNm}\right]$. Seven dynamic indexes to evaluate the changes of node voltage amplitude over the observation time are proposed and introduced as follows.

(1)　Percentage of voltage regulation time and Percentage of voltage over-limit time

Definition and Calculation 1. *The percentage of the node voltage amplitude regulation time refers to the percentage of data points whose relative error of the voltage amplitude measurement value to the average voltage measurement value is more than 2% in the present observation time window. Set N_{AT} as the number of the data points of voltage magnitude measurements beyond the "equivalent balance interval" in the present time observation window, then the voltage amplitude regulation time percentage at node j in the present observation time window is:*

$$U_{ATj} = \frac{N_{AT}}{N} \times 100\% \tag{6}$$

Similarly, the percentage of time that the node voltage exceeds the limits can be defined.

Definition and Calculation 2. *The percentage of the voltage over-limit time refers to the percentage of data points whose voltage amplitude measurement values are in the over-limit state in the present observation time window. Let N_{ET} represent the number of the data points of voltage magnitude measurements beyond the normal range over the rated voltage in the present time observation window. Thus, the voltage amplitude over-limit time percentage at node j in the present observation time window is calculated as follows:*

$$U_{ETj} = \frac{N_{ET}}{N} \times 100\% \tag{7}$$

(2)　Maximum fluctuation of voltage amplitude and maximum over-limit degree of voltage amplitude

Definition and Calculation 3. *The maximum fluctuation of voltage magnitude refers to the percentage of the difference between the maximum voltage measurement and minimum voltage measurement over the average voltage measurement. Assuming that the sampled data point number is labeled as i or l. The maximum fluctuation of voltage magnitude at node j in the present observation time window is written as:*

$$U_{MFj} = \begin{cases} \dfrac{\max\limits_{i,l=0,\cdots,N-1}\left|U_j(i)-U_j(l)\right|}{\overline{U}_j} \times 100\%, & \overline{U}_j \neq 0 \\ 0, & \overline{U}_j = 0 \end{cases} \tag{8}$$

Definition and Calculation 4. *The maximum over-limit degree of voltage amplitude refers to the maximum percentage of the value of the voltage magnitude measurement deviated from the normal range over the rated voltage, and is calculated as follows:*

$$U_{MEj} = \frac{\max\limits_{i=0,\cdots,N-1}\left\{U_j(i) - 1.05U_{jNm}, 0.95U_{jNm} - U_j(i), 0\right\}}{U_{jNm}} \times 100\% \tag{9}$$

(3) Voltage amplitude discrete intensity and Voltage over-limits intensity

The closer the node voltage amplitude dynamic trajectory is to the average value in its observation time window, or the closer it is to the upper and lower voltage bands, the better its dynamic characteristics. Based on this, this paper comprehensively considers the information of the two dimensions of amplitude and time and proposes two indicators as follows.

Definition and Calculation 5. *The voltage amplitude discrete intensity at node j in the present observation time window is displayed as follows:*

$$U_{DDj} = \begin{cases} \frac{1}{N}\sum\limits_{i=0}^{N-1}\left(\frac{|U_j(i)-\overline{U}_j|}{\overline{U}_j} \times 100\%\right), & \overline{U}_j \neq 0 \\ 0, & \overline{U}_j = 0 \end{cases} \tag{10}$$

Definition and Calculation 6. *The voltage amplitude over-limit intensity at node j in the present observation time window is displayed as follows:*

$$U_{EDj} = \frac{1}{NU_{jNm}}\left[\sum\limits_{i=0}^{N-1}\max\left(U_j(i) - 1.05U_{jNm}, 0\right) + \sum\limits_{i=0}^{N-1}\max\left(0.95U_{jNm} - U_j(i), 0\right)\right] \times 100\% \tag{11}$$

(4) Percentage of voltage amplitude fluctuation frequency

In dynamic systems, small inertia indicates that the state variables are prone to fluctuations. Considering this, in order to evaluate the "inertia" of the ADN, this paper defines the index of the percentage of voltage amplitude fluctuation frequency during the observation time window.

Definition and Calculation 7. *Percentage of voltage amplitude fluctuation frequency refers to the percentage of the actual total times for which the voltage amplitude curve crosses the "equivalent balance interval" over the theoretical maximum crossing times.*

Based on the discrete voltage amplitude measurements at node *j* in the present observation time window, the number of times the voltage amplitude dynamic trajectory traverses equivalent balance interval is recorded as N_{UP}, then the voltage amplitude fluctuation frequency percentage at node *j* in the observation time window is described as

$$U_{FFj} = \frac{N_{UP}}{N} \times 100\% \tag{12}$$

To calculate the value of N_{UP} in (12), the classification function $\boldsymbol{U}_{sj}$ is defined as

$$U_{Sj}(i) = \begin{cases} 1, & U_j(i) > 1.02\overline{U}_j \\ 0, & else \\ -1, & U_j(i) < 0.98\overline{U}_j \end{cases} \quad i = 0,1,2,\cdots,N \tag{13}$$

The calculation method of N_{UP} is summarized in Algorithm 1.

Algorithm 1 The Calculation Method of N_{UP}

1: Initialize i = 1, N_{UP} = 0
2: while i ≤ N − 1 do
3:    if $\left| U_{sj}(i+1) - U_{sj}(i) \right| \geq 1$ then
4:       $N_{UP} = N_{UP} + 1$;
5:          i = i + 1;
6:    end if
7: end while
8: Output $N_{UP} = N_{UP}$.

3.2.2. Dynamic Index of Individual Node Voltage Phase

The main grid is approximately regarded as an infinite system considering the ADN is connected to it through transformers and high-voltage distribution lines. Therefore, when the load or the DG output changes significantly in the ADN, the voltage phase of the related node will accordingly change non-steady at the same time. The non-steady voltage phase change described here is in terms of the steady phase change relatively.

The steady change of node voltage phase is defined as: in a relatively long length of the observation time window, the present angle frequency of node voltage $\overline{\omega}$ is obtained based on the frequency measurement data acquired by the PMUs, and the data sampling time interval is set as ΔT, then the steady change of node voltage phase is represented as $\Delta \overline{\varphi} = \overline{\omega} \cdot \Delta T$. Thus, if the voltage phase data at one node acquired by PMUs is deviated from $\Delta \overline{\varphi}$ beyond the set threshold, it is said that the voltage phase at this node occurs non-steady change.

It is indicated that the loads or DG outputs experience frequent impacts if the bus voltage phase often appears relatively significant non-steady changes. The more significant the impact is in the observation time window, the worse the dynamic characteristics of the ADN. On the other hand, if there is active power oscillation in the ADN in the observation window, the corresponding node voltage will occur non-steady change periodically. This kind of periodic non-steady change will also arise the periodic change of the voltage phase differences between different nodes.

Based on the aforementioned analysis, two indexes, i.e., the degree of voltage phase non-steady change and the maximum swing of voltage phase difference, are defined to indicate the impact loads and DG outputs as well as the degree of the active power oscillation in the ADN. Assume that there are N measurements for the voltage frequency f_j and absolute voltage phase $\varphi_j \in (0, 2\pi)$ at the node j in the observation time window, and the sampled data point number is noted as i, then the definition and calculation methods of these two indexes are as follows.

(1)   Degree of voltage phase non-steady change

Definition and Calculation 8. *The average frequency is represented by* $\overline{f}_j = \frac{1}{N} \sum\limits_{i=0}^{N-1} f_j(i)$, *and the steady change of the node voltage phase is marked as* $\Delta \overline{\varphi}_j = \mathrm{mod}(2\pi \overline{f}_j \cdot \Delta T, 2\pi)$. *When the voltage phase changes within the range* $\left[0.95 \Delta \overline{\varphi}_j, 1.05 \Delta \overline{\varphi}_j \right]$, *it is inferred that no non-steady change occurs. Thus, the degree of voltage phase non-steady change at node j in the observation time window is:*

$$
\begin{aligned}
U_{PDj} = \frac{1}{2\pi N} \sum_{i=0}^{N-1} \Big[&\max\Big(2\pi \eta_i + \varphi_j(i+1) - \varphi_j(i) - 1.05 \Delta \overline{\varphi}_j, 0 \Big) \\
&+ \max\Big(0.95 \Delta \overline{\varphi}_j - 2\pi \eta_i - \varphi_j(i+1) + \varphi_j(i), 0 \Big) \Big] \times 100\%
\end{aligned}
\tag{14}
$$

$$
\text{where, } \eta_i = \begin{cases} 0, & \varphi_j(i+1) - \varphi_j(i) \geq 0 \\ 1, & \varphi_j(i+1) - \varphi_j(i) < 0 \end{cases}
$$

(2)   Maximum swing of voltage phase difference

Definition and Calculation 9. *It is assumed that the node with the minimum value of the non-steady change degree in the whole network is numbered as s. Refer to node s, the voltage phase difference between node j and node s is represented as* $\Delta \varphi_{js}(i) = \varphi_j(i) - \varphi_s(i)$. *Thus, the maximum swing of voltage phase difference at node j in the present observation time window is described as follows.*

$$U_{PSj} = \begin{cases} \dfrac{\max\limits_{i=0,\cdots,N-1}[\Delta\varphi_{js}(i)] - \min\limits_{i=0,\cdots,N-1}[\Delta\varphi_{js}(i)]}{2\pi} \times 100\%, & j \neq s \\ 0, & j = s \end{cases} \tag{15}$$

3.3. Dynamic Index of Individual Branch

The most basic operating variable of a branch is current, but its power more intuitively describes the dynamic characteristics. Therefore, when defining the branch dynamic indexes, the focus is on the current amplitude over-limit situation and the power fluctuation situation during the dynamic process. Simultaneously, to evaluate the dynamic compensation capability of the reactive power compensation device and the reactive power adjustment function of DGs in ADN, a dynamic index regarding the branch power factor is proposed. Most of the definitions of branch dynamic index can be given by referring to node voltage dynamic indexes, which will not be repeated in this section. It should be noted that there may be bidirectional power flow in ADN, and the measured value of the backward power flow is expressed as minus, as shown in Figure 3b.

Assuming that the numbers of measurements of the current amplitude I_k, the active power P_k, the reactive power Q_k and the power factor F_k of branch k in the observation time window are N. The sampled data point number is noted as i. The average values of these four kinds of measurements are $\overline{I_k}, \overline{P_k}, \overline{Q_k}, \overline{F_k}$, respectively. The power limit of branch k is expressed as I_{km}. Then the indexes of branch k in the observation time window are:

(1)   Maximum over-limit degree of current

$$I_{MEk} = \frac{\max\limits_{i=0,\cdots,N-1}\{|I_k(i)| - I_{km}, 0\}}{I_{km}} \times 100\% \tag{16}$$

(2)   Current over-limit intensity

$$I_{EDk} = \frac{\sum\limits_{i=0}^{N-1} \max(|I_k(i)| - I_{km}, 0)}{N I_{km}} \times 100\% \tag{17}$$

(3)   Percentage of current fluctuation frequency

Definition and Calculation 10. *Percentage of current fluctuation frequency refers to the percentage of the actual total times for which the current curve crosses the "equivalent balance interval" over the theoretical maximum crossing times.*

Considering the bidirectional power flow, the average value of nonnegative measured values is recorded as $\overline{I}_k^+$, and the average value of negative measurements is denoted as $\overline{I}_k^-$. For dramatic fluctuation of branch current, the corresponding "equivalent balance interval +" is set as $\left[0.85\overline{I}_k^+, 1.15\overline{I}_k^+\right]$, while the "equivalent balance interval −" is set as $\left[0.85\overline{I}_k^-, 1.15\overline{I}_k^-\right]$. Based on the discrete current measurements of branch k in the present

observation time window, the number of times the current dynamic trajectory crosses the "equivalent balance interval (including the equivalent balance interval + and the equivalent balance interval −)" is recorded as N_{IP}, then the percentage of current fluctuation frequency of branch k in the observation time window is:

$$I_{FFj} = \frac{N_{IP}}{N} \times 100\% \tag{18}$$

The calculation method of N_{IP} is similar to N_{UP}, but the influence of the positive and negative measurement value needs to be considered as follows:

First, define the classification function I_{Sk} as:

$$I_{Sk}(i) = \begin{cases} 1, & I_k(i) > 1.15\overline{I}_k^+ \text{ or } I_k(i) < 1.15\overline{I}_k^- \\ 0, & else \\ -1, & 0 < I_k(i) < 0.85\overline{I}_k^- \text{ or } 0 > I_k(i) > 0.85\overline{I}_k^- \end{cases} \quad i = 0, 1, 2, \cdots, N \tag{19}$$

Apply I_{Sk} to clarify elements in $\{I_k(0), I_k(1), \cdots, I_k(N)\}^T$ one by one and obtain the one-dimensional classification vector $\{I_{Sk}(0), I_{Sk}(1), \cdots, I_{Sk}(N)\}^T$. Then the value of N_{IP} is as below:

$$\begin{aligned} N_{IP} &= \sum_{i=0}^{N-1} m_i \\ m_i &= \begin{cases} 1, & |I_{Sk}(i+1) - I_{Sk}(i)| \geq 1 \text{ or } I_k(i+1) \times I_k(i) < 0 \\ 0, & |I_{Sk}(i+1) - I_{Sk}(i)| = 0 \ \& \ I_k(i+1) \times I_k(i) >= 0 \end{cases} \end{aligned} \tag{20}$$

(4)   Active/Reactive power discrete intensity ($X = P$ or Q)

$$X_{DDk} = \begin{cases} \frac{1}{N} \sum_{i=0}^{N-1} \left(\left| \frac{X_k(i) - \overline{X}_k}{\overline{\overline{X}}_k} \right| \times 100\% \right), & \overline{X}_k \neq 0 \\ 0, & \overline{X}_k = 0 \end{cases} \tag{21}$$

3.4. Dynamic Comprehensive Index

After calculating each node's voltage dynamic index and each branch's dynamic index, the dynamic comprehensive indexes of node voltage and branch in the subareas and the whole ADN can be obtained.

(1)   Dynamic comprehensive index of subareas

According to the statistics of the dynamic indexes of all nodes in this subarea, the maximum and average values of the non-zero indexes are defined as two kinds of dynamic comprehensive indexes of the nodes, as shown in Table 2. Assuming that the total number of nodes in the present subarea is J. Taking the comprehensive index corresponding to U_{ATj} as an example, it is suggested that the voltage amplitude regulation time percentage of each node has been calculated and recorded in a one-dimensional vector $U_{AT} = (U_{ATj})_{J \times 1}$, and the total number of non-zero elements in U_{AT} is M. The set of these M nodes is represented by M_{node}, then the corresponding two types of subarea dynamic comprehensive indexes are shown as follows.

$$U_{AT\max}^{sub} = \max_{j \in M_{node}} U_{ATj} \tag{22}$$

$$\overline{U}_{AT}^{sub} = \frac{1}{M} \sum_{j \in M_{node}} U_{ATj} \tag{23}$$

Table 2. Dynamic comprehensive index set of node voltage.

Index Name		Subareas Index Expression	The Whole Network Index Expression
Dynamic comprehensive index set of node voltage			
Percentage of node voltage regulation time	Maximum	$U_{AT\max}^{sub}$	$U_{AT\max}$
	average	$\overline{U}_{AT}^{sub}$	$\overline{U}_{AT}$
Percentage of voltage over-limit time	Maximum	$U_{ET\max}^{sub}$	$U_{ET\max}$
	average	$\overline{U}_{ET}^{sub}$	$\overline{U}_{ET}$
Maximum fluctuation of voltage amplitude	Maximum	$U_{MF\max}^{sub}$	$U_{MF\max}$
	average	$\overline{U}_{MF}^{sub}$	$\overline{U}_{MF}$
Maximum over-limit degree of voltage amplitude	Maximum	$U_{ME\max}^{sub}$	$U_{ME\max}$
	average	$\overline{U}_{ME}^{sub}$	$\overline{U}_{ME}$
Voltage amplitude discrete intensity	Maximum	$U_{DD\max}^{sub}$	$U_{DD\max}$
	average	$\overline{U}_{DD}^{sub}$	$\overline{U}_{DD}$
Voltage over-limits intensity	Maximum	$U_{ED\max}^{sub}$	$U_{ED\max}$
	average	$\overline{U}_{ED}^{sub}$	$\overline{U}_{ED}$
Percentage of voltage amplitude fluctuation frequency	Maximum	$U_{FF\max}^{sub}$	$U_{FF\max}$
	average	$\overline{U}_{FF}^{sub}$	$\overline{U}_{FF}$
Degree of voltage phase non-steady change	Maximum	$U_{PD\max}^{sub}$	$U_{PD\max}$
	average	$\overline{U}_{PD}^{sub}$	$\overline{U}_{PD}$
Maximum swing of voltage phase difference	Maximum	$U_{PS\max}^{sub}$	$U_{PS\max}$
	average	$\overline{U}_{PS}^{sub}$	$\overline{U}_{PS}$
Dynamic comprehensive index set of branch			
Maximum current over-limit	Maximum	$I_{ME\max}^{sub}$	$I_{ME\max}$
	average	$\overline{I}_{ME}^{sub}$	$\overline{I}_{ME}$
Current over-limit intensity	Maximum	$I_{ED\max}^{sub}$	$I_{ED\max}$
	average	$\overline{I}_{ED}^{sub}$	$\overline{I}_{ED}$
Percentage of current fluctuation frequency	Maximum	$I_{FF\max}^{sub}$	$I_{FF\max}$
	average	$\overline{I}_{FF}^{sub}$	$\overline{I}_{FF}$
Active power discrete intensity	Maximum	$P_{DD\max}^{sub}$	$P_{DD\max}$
	average	$\overline{P}_{DD}^{sub}$	$\overline{P}_{DD}$
Reactive power discrete intensity	Maximum	$Q_{DD\max}^{sub}$	$Q_{DD\max}$
	average	$\overline{Q}_{DD}^{sub}$	$\overline{Q}_{DD}$

If the value of an index at all nodes in this subarea is zero, then M_{node} is an empty set, and the corresponding maximum index and average index are both zero.

Similar to the node voltage dynamic comprehensive index, two types of dynamic comprehensive indexes of the branch dynamics in subareas can be defined, as shown in Table 2.

(2) Dynamic comprehensive index of the whole network

For the whole network, there are also two categories of dynamic comprehensive indexes, i.e., the maximum category and the average category, as presented in Table 2. The calculation method of these indexes is similar to the subareas indexes.

According to Table 2, there are 30 indexes in the subareas evaluation index system and the whole network evaluation index system, respectively, which can be used to diagnose over-limit, short-time impact, and oscillation. The value of these indexes can characterize the severity of the corresponding adverse dynamics. All indexes' values range between [0%, 100%] and can be compared mutually. In practical application, the corresponding set of indexes can be flexibly selected according to the assessment needs. This is the reason for constructing a 'redundancy' index system.

4. Real-Time Dynamic Behavior Evaluation Methodology of ADNs

The application of the low-cost PMU proposed in Section 2 can satisfy the observability requirements of the active distribution network at an acceptable cost. On this basis, the dynamic indexes of each bus and branch can be calculated directly from the PMU data so as to describe their dynamic characteristics. However, for assessing the dynamic characteristics of the whole network, a comprehensive analysis is required, which is described in detail below.

4.1. Causes and Severity Evaluation Methods of Adverse Dynamic Behaviors

As mentioned in Section 3, the indexes can be used to identify adverse dynamics including over-limit, short-time impact, and oscillation. For instance, create a subset of indexes for diagnosis of over-limit $\{X_{ET\max}^{sub}, X_{ET\max}, \overline{X}_{ET}^{sub}, \overline{X}_{ET}, X_{ME\max}^{sub}, X_{ME\max}, \overline{X}_{ME}^{sub}, \overline{X}_{ME}, X_{ED\max}, \overline{X}_{ED}\}$ (X represents U, I). If there is any non-zero element in this subset, it indicates that there is an over-limit situation during the present observation time window. If the index subset $\{X_{MF\max}, \overline{X}_{MF}\}$ has elements with large values and the value of all the elements in the index subset $\{X_{FF\max}, \overline{X}_{FF}\}$ are small, the network may suffer a short-time impact. And if the index values of both subsets are large, oscillation may exist in the network. To further judge short-time impacts and oscillations (multiple impacts are considered as forced oscillations), the analysis needs to be performed in conjunction with PMU data from multiple adjacent observation time windows, as described in Section 5.

4.2. Comprehensive Assessment of Dynamic Characteristics for Subareas and for the Whole Network

To intuitively characterize the overall dynamic characteristics of a specific subarea, the corresponding comprehensive assessment index is defined.

Assume that in the evaluation process, S_1, S_2, and S_3 indicators are selected for the subset of over-limit indexes, oscillation indexes and short-time impact indexes, respectively. Considering the different severity of the impact on the system when these three adverse dynamics occur, the corresponding weights are set to 0.4, 0.4, and 0.2, respectively (the weights can be adjusted appropriately in practical applications). Then, the comprehensive assessment index of the dynamic characteristics for the subarea is as follows.

$$C_I^{sub} = \frac{0.4}{S_1}\sum_{i=1}^{S_1} I_{Ni}^{sub} + \frac{0.4}{S_2}\sum_{i=S_1+1}^{S_1+S_2} I_{Ni}^{sub} + \frac{0.2}{S_3}\sum_{i=S_1+S_2+1}^{S_1+S_2+S_3} I_{Ni}^{sub} \tag{24}$$

where I_{Ni}^{sub} represents the value of the i-th index.

The calculation method of the comprehensive dynamic characteristic evaluation index of the whole network C_I is the same as that of the subarea and only differs in the number of nodes involved.

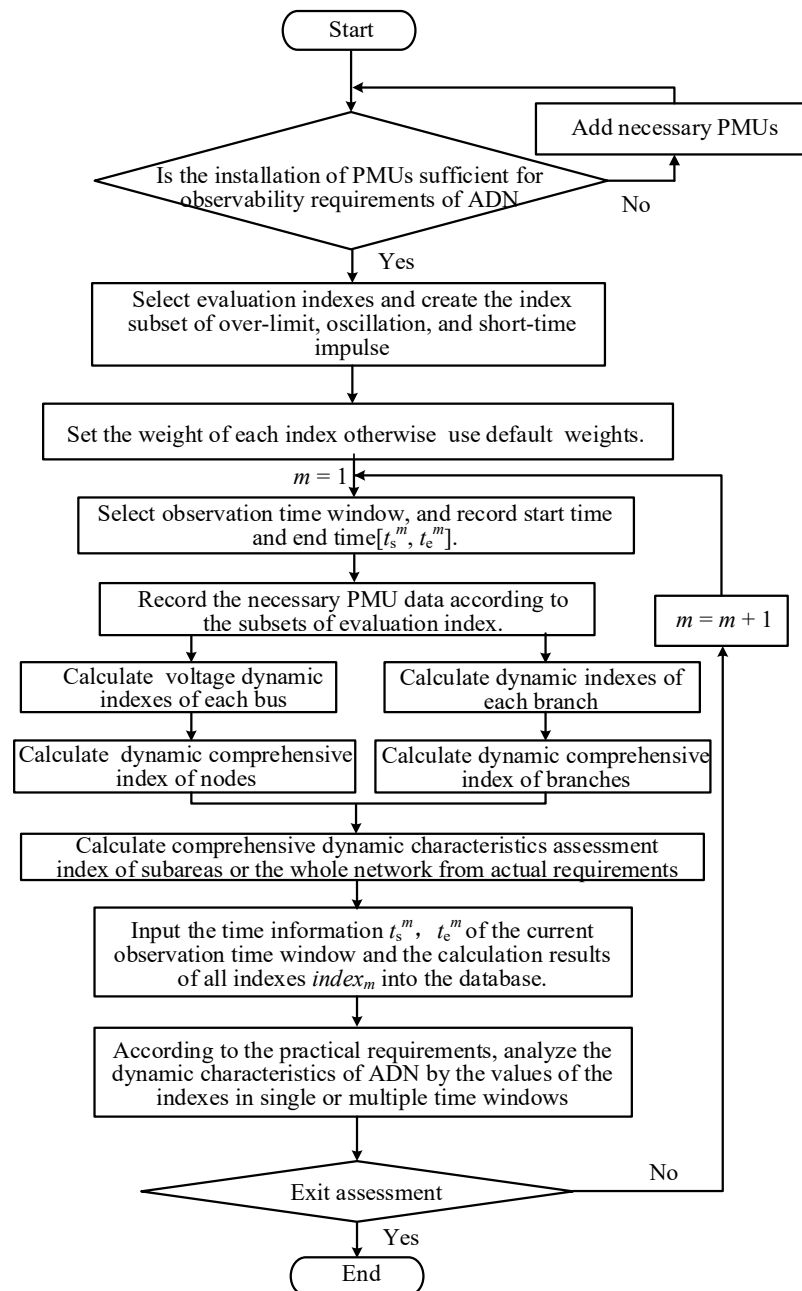The flow chart of the real-time dynamic behavior evaluation for ADN is displayed in Figure 4.

Figure 4. Flow chart of real-time dynamic behavior evaluation for ADN.

5. Case Study

In order to verify the practicability and effectiveness of the proposed dynamic characteristic evaluation method, a numerical test is carried out on the modified IEEE 123-bus distribution network shown in Figure 5. This system has 123 nodes and 122 branches, which is comparable to a real regional distribution network. The voltage magnitude of the substation bus is set to be 10.5 kV as a reference, and the upper and the lower voltage limits for each bus are set to be 1.05 p.u. and 0.95 p.u., respectively. The network is partition into three subareas based on the distance to the reference node, with subarea 2 being the EV charging zone and subarea 3 being the DG demonstration zone. Both EV charging stations and DGs have two types and are labeled separately. In this paper, all DGs and loads are simulated as having a constant power factor.
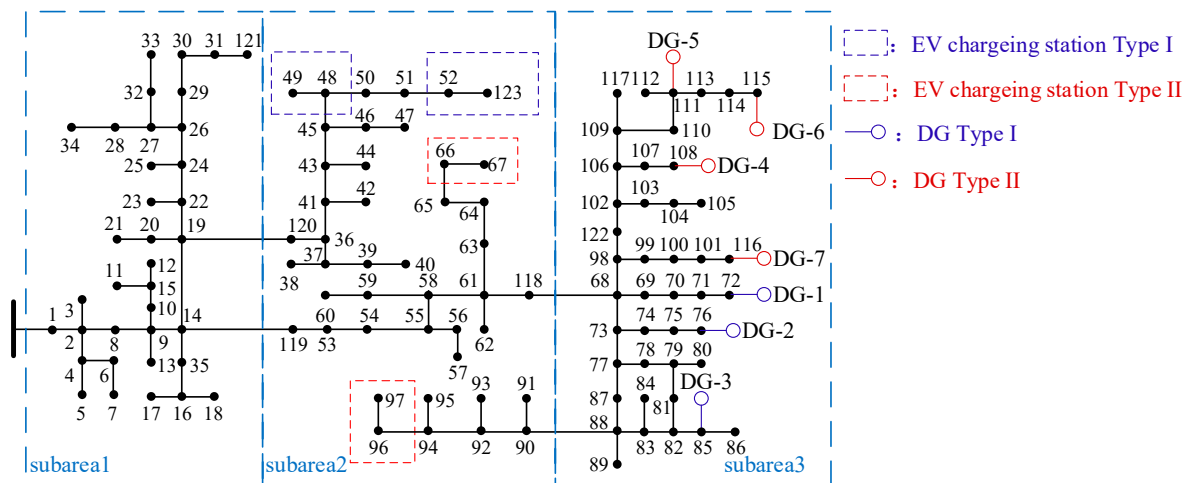
Figure 5. The modified IEEE 123-bus distribution network.

The installed capacities of DG-1 to DG-7 are 0.5, 1.3, 0.68, 0.48, 1.42, 0.71, 1.08 MW, respectively. The forecasting output of each DG unit is 50% of the installed capacity, and the random forecasting error fluctuates according to the Laplace distribution, within the limit of [0, installed capacity]. Based on the DG output as the benchmark and changing the standard deviation of Laplace distribution, two types of actual DG output curves can be obtained, as shown in Figure 6a. For buses with uncertain load, the corresponding actual load demand curves with the benchmark of the standard load are obtained as shown in Figure 6b. According to the results in Table 1, the error of PMU measurement data is set to be 0.2%. The error is modeled as Gaussian variance and added to the measurements. The other detailed parameters of the network are from references [26,27].
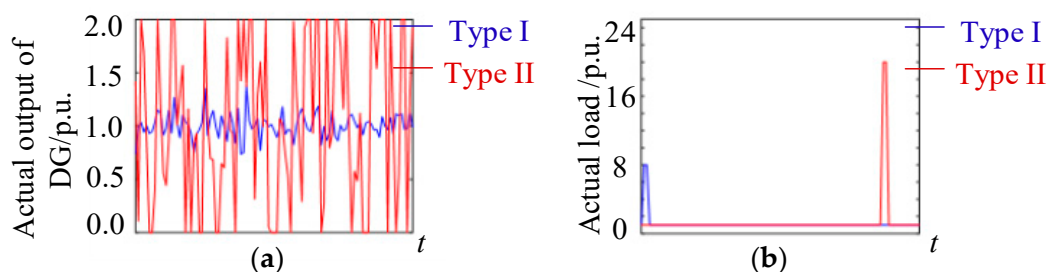

Figure 6. The DG output and load demand curves: (**a**) Actual DG output; (**b**) Actual load demand.

5.1. Online Dynamic Characteristics Assessment in a Single Time Window

Assuming that there is one sampling point in one frequency period, the observation time window length is 2 s. According to the flow shown in Figure 4, indicators are selected to construct the subsets of the over-limit index, oscillation index, and short-time impact index, and the dynamic characteristics indexes of the whole network in the 1st time window are solved and listed in Table 3.

Table 3. Online dynamic characteristics assessment in a single time window.

Over-Limit Index	Value	Oscillation Index	Value	Short-Time Impact Index	Value
$U_{ET\max}$	0	$\overline{U}_{DD}$	0.5064	$U_{MF\max}$	3.3281
$\overline{U}_{ME}$	0	$U_{FF\max}$	2	$\overline{U}_{MF}$	2.1896
$U_{ED\max}$	0	$\overline{U}_{FF}$	2	$U_{ME\max}$	0
$\overline{I}_{ME}$	0	$I_{FF\max}$	74	$I_{ME\max}$	0
$\overline{I}_{ED}$	0	$\overline{I}_{FF}$	44.4		
C_I	10.1084				

Among them, the maximum values of indexes $\{U_{FF\max}, U_{MF\max}\}$ appear at bus $\{43, 115\}$, respectively. The maximum values of indexes $\{I_{FF\max}, I_{ME\max}\}$ appear at branches $\{14\text{–}119, 1\text{–}2\}$ (if the maximum value of index appears at multiple nodes or branches, the minimum number is counted as the solution). Combined with the above information, the analysis is shown as follows:

(1) The value of indexes in the over-limit index subset are zero, so there is no over-limit situation in the network in the 1st time window.

(2) Check the values in oscillation index subset and short-term impact index subset. For the dynamic index of node voltage, the maximum value of $U_{FF\max}$ comes from bus-43, reflecting the influence of the impact loads around; the maximum value of $U_{MF\max}$ appears at bus-115, indicating that this index is mainly affected by the fluctuation of DG-6 output. For branch dynamic indexes, $I_{FF\max}$ occurs in branch 14–119, while $I_{ME\max}$ appears in branch 1–2, both reflects the variation of the power delivered from this branch to the nodes behind.

(3) C_I of the whole network is 10.1084, which indicates that the dynamic characteristics of this network in the present time window is relatively acceptable but can still be optimized.

5.2. Online Dynamic Characteristics Evaluation on Moving Time Window

The dynamic characteristics of this distribution system are evaluated in 10 consecutive moving time windows with the step length of 1 s. The over-limit index subset, oscillation index subset, and short-time impact index subset are consistent with Section 5.1. The numerical curves of some typical indexes (including subarea indexes and the whole network indexes) are plotted in Figure 7, which show that:

(1) The comprehensive dynamic characteristic index for the whole network is influenced by the coupling of the three zones with each other, and always follows the worst situation among subareas.

(2) The non-zero values of over-limit index $U_{ME\max}$ and short-time impact index $U_{ET\max}$, $I_{ME\max}$ all appear in the last two time windows. It is clear that the former two follow the impact in subarea 2, while the latter one comes from subarea 1. However, $I_{ME\max}$ appears at branch 1–2 during the entire observation period, which reflects the electricity from utility grid to this network to satisfy its load demand. Thus, the non-zero values of all these three indexes are due to the influence of load impact in subarea 2.

(3) $I_{FF\max}$ is not zero but $I_{ME\max}$ remains zero in the first eight time windows. A comparison of these two indexes shows that the fluctuations of $I_{FF\max}$ in the first eight time windows are mainly due to the bidirectional power flow caused by stochastic DG output. However, this fluctuation does not result in the over-limit of current. Comparing the values of $U_{ME\max}$ and $U_{MF\max}$ together with their changes leads to the same conclusion.

(4) The value of C_I increases significantly in the 9th time window, reflecting the influences of the impact loads at subarea 2. It then decreases slightly in the 10th time window, which, combined with the fluctuating trend of $I_{FF\,\max}^{sub}$, can be seen as a result of the fluctuation of DG output slowing down in the 10th window.

The assessment results in different subareas of the modified IEEE 123-bus network show that the proposed assessment method is not dependent on a particular topology or a particular operation mode of the active distribution network and is highly adaptable. Moreover, it is worth noting that for ADN in large zones, the comprehensive dynamic characteristic index for subareas can quickly suggest areas where adverse dynamic triggers are likely to be located.
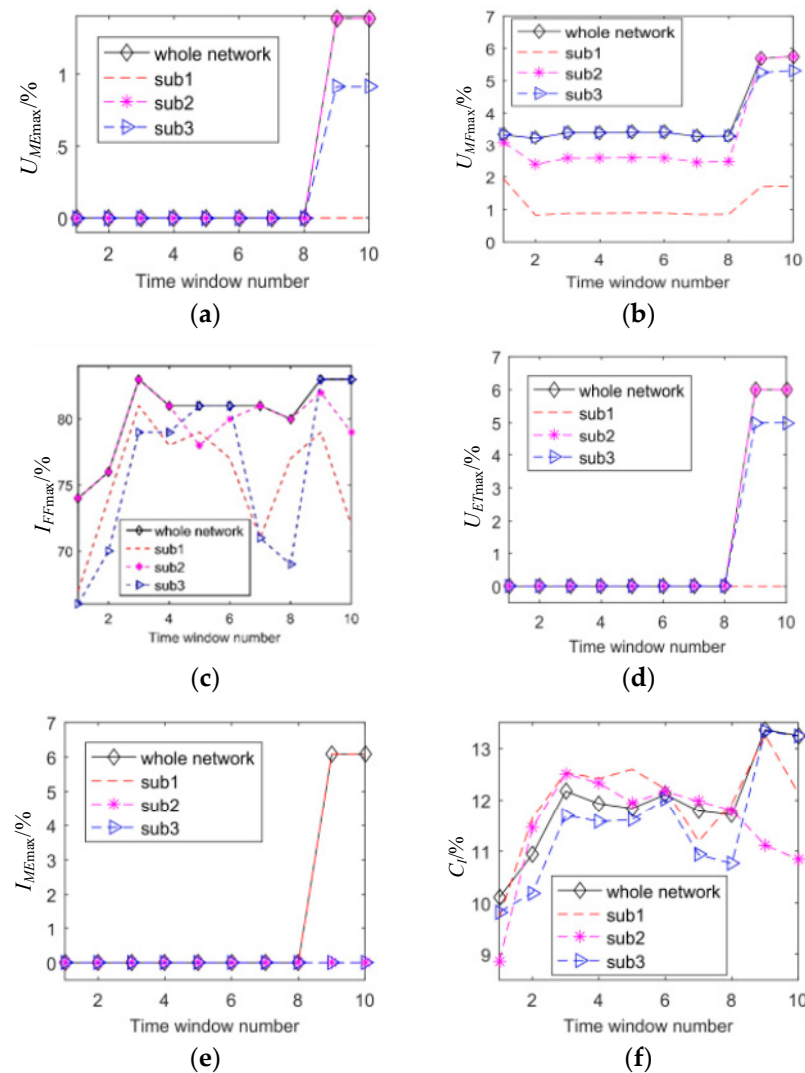
Figure 7. Comprehensive dynamic characteristic index curves in the modified IEEE 123-bus network:
(**a**) Maximum over-limit degree of voltage amplitude; (**b**) maximum node voltage amplitude fluctuations;
(**c**) percentage of the branch current fluctuation frequency; (**d**) percentage of voltage over-limit time;
(**e**) maximum branch current over-limit; (**f**) comprehensive dynamic characteristics evaluation index.

6. Conclusions

This paper proposes a novel method based on low-cost PMUs to evaluate the real-time dynamic behavior of active distribution networks. The proposed evaluation model encompasses the assessment principles of accuracy, integrity, practicability, and adaptability. In addition, it is proved that the presented assessment methodology is applicable to compare the dynamic characteristics of distribution networks before and after performing various operation modes, coordinated control, and network reconfiguration. Similarly, in terms of the ADN planning aspect, the proposed approach offers reference indexes for installing equipment and optimizing network structure. Finally, the innovative features of the proposed real-time dynamic characteristics assessment method are listed as follows:

- Introduce low-cost PMUs implementation for the real-time dynamic behavior evaluation of active distribution networks.
- The proposal of a non-DFT-based methodology for low-cost PMUs can satisfy the observability requirements of ADNs at an acceptable cost.
- Establish a dynamic index system to manifest the dynamic changes of node voltage amplitude, node voltage phase, and branch power flow based on PMU data, following a multi-level progression of node-branch-subarea-network.

- Various adverse dynamic behaviors of ADN such as over-limits, oscillation, short-time impact, are considered in the proposed scheme. In addition, a detailed dynamic characteristic evaluation process is presented and demonstrated.
- The validation of the proposed model was performed using a modified IEEE 123-bus network, and the obtained results prove the applicability and effectiveness of the proposed method.

References

1. Ehsan, A.; Yang, Q. State-of-the-Art Techniques for Modelling of Uncertainties in Active Distribution Network Planning: A Review. *Appl. Energy* **2019**, *239*, 1509–1523. [CrossRef]
2. Li, Z.; Su, S.; Jin, X.; Chen, H.; Li, Y.; Zhang, R. A Hierarchical Scheduling Method of Active Distribution Network Considering Flexible Loads in Office Buildings. *Int. J. Electr. Power Energy Syst.* **2021**, *131*, 106768. [CrossRef]
3. Li, Y.; Feng, B.; Li, G.; Qi, J.; Zhao, D.; Mu, Y. Optimal Distributed Generation Planning in Active Distribution Networks Considering Integration of Energy Storage. *Appl. Energy* **2018**, *210*, 1073–1081. [CrossRef]
4. Swain, K.P.; De, M. A Novel Electrical Proximity Index for Voltage Control in Smart Distribution System. *Electr. Power Syst. Res.* **2019**, *172*, 50–62. [CrossRef]
5. Sun, C.; Mi, Z.; Ren, H.; Jing, Z.; Lu, J.; Watts, D. Multi-Dimensional Indexes for the Sustainability Evaluation of an Active Distribution Network. *Energies* **2019**, *12*, 369. [CrossRef]
6. Zhai, H.F.; Yang, M.; Chen, B.; Kang, N. Dynamic Reconfiguration of Three-Phase Unbalanced Distribution Networks. *Int. J. Electr. Power Energy Syst.* **2018**, *99*, 1–10. [CrossRef]
7. Notton, G.; Nivet, M.-L.; Voyant, C.; Paoli, C.; Darras, C.; Motte, F.; Fouilloy, A. Intermittent and Stochastic Character of Renewable Energy Sources: Consequences, Cost of Intermittence and Benefit of Forecasting. *Renew. Sustain. Energy Rev.* **2018**, *87*, 96–105. [CrossRef]
8. Hasankhani, A.; Hakimi, S.M. Stochastic Energy Management of Smart Microgrid with Intermittent Renewable Energy Resources in Electricity Market. *Energy* **2021**, *219*, 119668. [CrossRef]
9. Ullah, Z.; Wang, S.; Radosavljević, J.; Lai, J. A Solution to the Optimal Power Flow Problem Considering WT and PV Generation. *IEEE Access* **2019**, *7*, 46763–46772. [CrossRef]
10. Chen, Y.; Sun, J.; Zha, X.; Yang, Y.; Xu, F. A Novel Node Flexibility Evaluation Method of Active Distribution Network for SNOP Integration. *IEEE J. Emerg. Sel. Top. Circuits Syst.* **2021**, *11*, 188–198. [CrossRef]
11. Yang, H.; Qiu, R.C.; Tong, H. Reconstruction Residuals Based Long-Term Voltage Stability Assessment Using Autoencoders. *J. Mod. Power Syst. Clean Energy* **2020**, *8*, 1092–1103. [CrossRef]
12. A Survey of Reliability Assessment Techniques for Modern Distribution Networks—ScienceDirect. Available online: https://www.sciencedirect.com/science/article/pii/S1364032118300650?via%3Dihub (accessed on 31 May 2021).
13. Escalera, A.; Prodanović, M.; Castronuovo, E.D. Analytical Methodology for Reliability Assessment of Distribution Networks with Energy Storage in Islanded and Emergency-Tie Restoration Modes. *Int. J. Electr. Power Energy Syst.* **2019**, *107*, 735–744. [CrossRef]
14. Zhao, H.S.; Liu, H.Y.; Chen, S.; Wang, Y.Y.; Zhao, H.Y. Reliability Assessment of Distribution Network Considering Preventive Maintenance. In Proceedings of the 2016 IEEE Power and Energy Society General Meeting (PESGM), Boston, MA, USA, 17–21 July 2016; pp. 1–5.
15. Zhou, L.; Li, F.; Gu, C.; Hu, Z.; Blond, S.L. Cost/Benefit Assessment of a Smart Distribution System with Intelligent Electric Vehicle Charging. *IEEE Trans. Smart Grid* **2014**, *5*, 839–847. [CrossRef]
16. Tao, W.; Ma, M.; Ding, M.; Xie, W.; Fang, C. A Priority-Based Synchronous Phasor Transmission Protocol Extension Method for the Active Distribution Network. *Appl. Sci.* **2019**, *9*, 2135. [CrossRef]

17. von Meier, A.; Stewart, E.; McEachern, A.; Andersen, M.; Mehrmanesh, L. Precision Micro-Synchrophasors for Distribution Systems: A Summary of Applications. *IEEE Trans. Smart Grid* **2017**, *8*, 2926–2936. [CrossRef]
18. Mayo-Maldonado, J.C.; Valdez-Resendiz, J.E.; Guillen, D.; Bariya, M.; von Meier, A.; Salas-Esquivel, E.A.; Ostfeld, A. Data-Driven Framework to Model Identification, Event Detection, and Topology Change Location Using D-PMUs. *IEEE Trans. Instrum. Meas.* **2020**, *69*, 6921–6933. [CrossRef]
19. Xiao, M.; Wang, S.; Ullah, Z.; Li, Y.; Arghandeh, R. Reza Arghandeh Topology Detection in Power Distribution System Using Kernel-Node-Map Deep Networks. *IET Gener. Transm. Distrib.* **2020**, *14*, 4033–4041. [CrossRef]
20. Puddu, R.; Brady, K.; Muscas, C.; Pegoraro, P.A.; Von Meier, A. PMU-Based Technique for the Estimation of Line Parameters in Three-Phase Electric Distribution Grids. In Proceedings of the 2018 IEEE 9th International Workshop on Applied Measurements for Power Systems (AMPS), Bologna, Italy, 26–28 September 2018; pp. 1–5.
21. Zhang, Y.; Wang, J.; Khodayar, M.E. Graph-Based Faulted Line Identification Using Micro-PMU Data in Distribution Systems. *IEEE Trans. Smart Grid* **2020**, *11*, 3982–3992. [CrossRef]
22. Xiao, M.; Wang, S.; Ullah, Z. D-PMU and 5G-Network-Based Coordination Control Method for Three-Phase Imbalance Mitigation Units in the LVDN. *Energies* **2021**, *14*, 2754. [CrossRef]
23. Angioni, A.; Lipari, G.; Pau, M.; Ponci, F.; Monti, A. A Low Cost PMU to Monitor Distribution Grids. In Proceedings of the 2017 IEEE International Workshop on Applied Measurements for Power Systems (AMPS), Liverpool, UK, 20–22 September 2017; pp. 1–6.
24. Zhao, J.; You, S.; Yin, H.; Tan, J.; Liu, Y. Data Quality Analysis and Solutions for Distribution-Level PMUs. In Proceedings of the 2019 IEEE Power Energy Society General Meeting (PESGM), Atlanta, GA, USA, 4–8 August 2019; pp. 1–5.
25. Wang, S. A Distributed Wide-Area Synchronized Parallel Processing Platform for Power System Monitoring and Control. Ph.D. Thesis, University of Science and Technology (HUST), Wuhan, China, 2004.
26. Xin, C.; Wu, W.; Zhang, B. Data-Driven DG Capacity Assessment Method for Active Distribution Networks. *IEEE Trans. Power Syst.* **2017**, *32*, 3946–3957.
27. Wang, J.; Zhu, X.; Lubkeman, D.; Lu, N.; Samaan, N.; Werts, B. Load Aggregation Methods for Quasi-Static Power Flow Analysis on High PV Penetration Feeders. In Proceedings of the 2018 IEEE/PES Transmission and Distribution Conference and Exposition (T D), Denver, CO, USA, 16–19 April 2018; pp. 1–5.